PAPER

Check for updates

Novel onboard ammonia cracker for light-duty automotive fuel cell vehicles†

Chidozie Eluwah [iD] [ab] and Paul S. Fennell[a]

This work introduces an innovative onboard ammonia cracker module integrated with a 100-kW fuel cell system for light-duty automotive fuel cell vehicles. Utilizing a hollow fibre palladium membrane reactor (HFMR), two configurations are explored: a 3 × 3 simultaneous heating and cracking module and a 4 × 4 intermediate heating and cracking module. The 3 × 3 module, arranged in a serpentine configuration, exhibits superior performance with a calculated required volume of 8.9 liters, a total module area of 1.2 m^2 and a process thermal efficiency of 93.5%. Each reactor in this module operates isothermally at an exit temperature of 475 °C, achieving ammonia conversion rates that increase from 15.8% in the first reactor (R1) to an impressive 99.99% in the final reactor (R8), facilitated by *in situ* hydrogen removal through the palladium membrane. The steady-state analysis was carried out using Aspen Plus Software, and validated against experimental data from existing literature. The results demonstrated a high degree of agreement, confirming the model's capability to accurately predict system performance. For transient analysis, Aspen Plus Dynamics was employed to assess the system's responsiveness to varying driving conditions. Utilizing the Hyundai Nexo fuel cell car as a case study, the worldwide harmonised light vehicle test procedure (WLTP) was simulated, to model realistic driving cycles, allowing for a rigorous interrogation of the transient performance of the on-board ammonia cracker. Overall, this research establishes a 3 × 3 simultaneous heating and cracking HFMR module as the optimal configuration for on-board ammonia cracking for hydrogen production in fuel-cell vehicles, highlighting its operational efficiency and potential contribution to sustainable transportation solutions. Future research should focus on optimizing heat management and temperature control within the HFMR module, as well as enhancing transient response characteristics and ammonia safety, to boost system performance and support the wider implementation of hydrogen technologies in the automotive industry.

1. Introduction

The transportation sector heavily depends on fossil fuels, contributing significantly to global warming, air pollution, and the depletion of the ozone layer. According to the U.S. Energy Information Administration (EIA), the transportation sector accounted for 30.9% of carbon dioxide emissions in 2014.[1] Fig. 1 illustrate carbon dioxide emissions across various sectors in recent years, with projections for future emissions also shown. In response to these environmental concerns, the development of sustainable transportation technologies has become essential (EVs).[2] EVs have emerged as a key solution to reducing greenhouse gas emissions and improving air quality.[3] Their advantages, such as zero tailpipe emissions and lower operational costs, make them a cornerstone in efforts to combat climate change.

However, despite their promising potential, EVs face significant challenges, particularly with regard to the availability of charging infrastructure and limitations in battery technology.[4] A key issue is the prolonged charging time required to recharge EV batteries, which contrasts sharply with the quick refuelling of conventional internal combustion engine vehicles.[5] This inconvenience often leads to range anxiety and limits the practicality of EVs for long-distance travel.[6] The average time to fully charge an EV battery can range from 30 minutes to several hours, depending on the charging infrastructure.[7] While fast chargers can mitigate this issue to some extent, they are not universally available, and even fast charging can take 30 minutes or more to achieve an 80% charge.[8,9] This extended downtime, coupled with the uneven distribution of charging stations, particularly in rural or underserved areas, poses a barrier to widespread EV adoption.[2,10]

Hydrogen fuel cell vehicles (FCVs) offer a compelling alternative to address the charging challenges faced by battery electric vehicles (EVs). Unlike EVs, which require lengthy charging sessions, FCVs can be refuelled in a matter of minutes at a hydrogen refuelling station, similar to traditional gasoline or

a Department of Chemical Engineering, South Kensington Campus, Imperial College London, London SW7 2AZ, UK

b Unconventional Resource Production Department, Saudi Arabian Oil Company

† Electronic supplementary information (ESI) available. See DOI: https://doi.org/10.1039/d4ya00601a

Carbon Dioxide Emissions
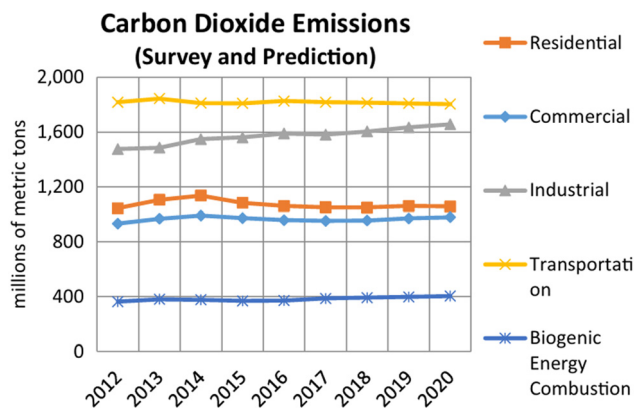### (Survey and Prediction)

Fig. 1   Emission statistics of carbon dioxide in different sectors (adopted from ref. 1).

diesel vehicles.[11] This rapid refuelling capability significantly reduces downtime and enhances the convenience of using FCVs for both short trips and long-distance travel.[12,13] Fuel cell vehicles generate electricity through an electrochemical reaction between hydrogen and oxygen, with water as the only byproduct.[14] The hydrogen is stored in high-pressure tanks within the vehicle, and the refuelling process involves transferring hydrogen into these tanks, typically taking less than 10 minutes.[15,16] This quick refuelling process helps overcome one of the main challenges of battery electric vehicles, providing a practical alternative for those concerned about longer recharge times.[9] Hydrogen fuel cell vehicles (FCVs) offer significant promise but face notable challenges, particularly concerning hydrogen storage and refuelling infrastructure. The main obstacles to adopting on-board hydrogen (H_2) storage systems for automotive applications include hydrogen's low volumetric energy density and associated safety concerns. These challenges hinder the practical use of hydrogen as a fuel source and highlight the need for alternative carriers that support efficient, cost-effective storage and transportation.

Due to its low energy density by volume, hydrogen requires advanced storage solutions. The two primary methods—high-pressure storage at around 70 000 kPa and cryogenic storage at extremely low temperatures—both present technical hurdles. High-pressure storage demands robust, heavy tanks to safely contain hydrogen, while cryogenic storage requires substantial energy input to maintain hydrogen in its liquid form.[9,13,17,18] Both approaches are complex and energy intensive. In addition to storage challenges, the development of hydrogen refuelling stations presents further obstacles, including safety concerns, logistical issues in storage and transportation, and the relative immaturity of the technology. As of 2024, there are fewer than 600 hydrogen refuelling stations globally, with the majority located in Europe, Japan, and California.[19] This limited infrastructure, in contrast to the extensive network of electric vehicle (EV) charging stations, hinders the widespread adoption of FCVs and creates a significant accessibility gap.[20]

The search for alternative fuels to support the transition to cleaner transportation technologies has led to significant interest in ammonia (NH_3) as a potential hydrogen carrier. Recent research has explored ammonia's dual role as both a hydrogen carrier and energy storage medium, with a particular focus on its potential in combustion engines and fuel cells. Compared to hydrogen, ammonia can be stored and transported more efficiently.[21,22] Studies by the international renewable energy agency (IRENA)[23] further highlight ammonia's economic advantages for long-distance transport, citing its low conversion costs and minimal impact from transportation distance. Ammonia presents a highly promising alternative fuel, offering significant advantages due to its high energy density, ease of liquefaction, and safer storage compared to hydrogen. With a volumetric energy density of 2916.7 W h L^{-1} at room temperature and approximately 800 kPa, ammonia's storage efficiency is more than double that of compressed hydrogen at 70 000 kPa, which has a volumetric energy density of 1388.9 W h L^{-1}.[24] Additionally, ammonia boasts a high hydrogen gravimetric density of 17.8% by weight and a superior volumetric hydrogen density of 123 kg-H_2 per m^3 at 1 MPa. This makes ammonia a more efficient storage medium compared to other options such as metal hydrides (25 kg-H_2 per m^3), liquefied hydrogen (71 kg-H_2 per m^3), and methanol (99 kg-H_2 per m^3).[25–27] Moreover, ammonia benefits from an established infrastructure for production, storage, and distribution, positioning it as a highly viable alternative fuel in the ongoing transition to cleaner transportation technologies.

Ammonia is primarily synthesized through the Haber–Bosch process, which combines nitrogen and hydrogen under high pressure and temperature. Recent advancements in green ammonia production leverage renewable energy sources for hydrogen generation, as reported by Gordon et al.[28] In addition, advancements in storage technologies, including ammonia-based chemical hydrides, have been explored to enhance ammonia's utility in automotive applications.[29] Ammonia cracking is crucial for converting ammonia into hydrogen, which is then used in fuel cells. Effective cracking systems must achieve high ammonia conversion rates while managing energy consumption, catalyst durability, safety, and by-products like nitrogen oxides (NOx).[30] In a previous publication,[31] we introduced our innovative hybrid air-volt ammonia cracker (HAVAC) process. This process seamlessly integrates renewable electricity with autothermal operation to efficiently crack blue or green ammonia. It achieves exceptional thermal efficiency (94%–95%) and demonstrates ammonia conversion rates of up to 99.4%, with hydrogen yields between 84% and 99.5%. The resultant hydrogen purity reaches 99.99%, meeting ISO 14687:2019 standards. However, this process is designed for centralized ammonia cracking and does not address onboard ammonia cracking applications.

Mazzone et al.[32] experimentally compared hollow fibre and packed bed reactors for onboard hydrogen production via ammonia cracking. Their findings revealed that hollow fibre reactors are substantially more efficient, offering a 4.6-fold increase in ammonia cracking rate, a 99% reduction in pressure drop, and requiring 80% less volume and catalyst compared to packed bed reactors. Specifically, the hollow fibre reactor needs 11 liters of volume and 3.5 kg of catalyst for 100 kW of hydrogen

power, *versus* 54 liters and 16.2 kg for the packed bed reactor. Despite the advantages, challenges remain in catalyst deactivation, uniform catalyst distribution, reactor design, compactness, and integration with fuel cell engines. Lingling Zhai *et al.*,[33] through a laboratory experiment, developed and demonstrated an innovative NH_3-powered fuel cell electric golf cart as a proof of concept for NH_3-based fuel cell vehicles. The system integrates an NH_3 cracker with a catalyst, a gas purifier, a fuel cell, and an energy management system. The researchers tested various Ni and Fe-based catalysts, with a Ru-modified Ni catalyst achieving over 99.9% NH_3 conversion at 600 °C. The resulting gas mixture, consisting of 75% H_2 and 25% N_2, was purified using a regenerable zeolite-based gas purifier to ensure compatibility with the proton exchange membrane fuel cell (PEMFC). The system powered 300 W and 600 W fuel cells, demonstrating sufficient energy output to propel the golf cart over 500 km at 25 km h^{-1}. The energy system achieved a specific energy of 379.4 W h kg^{-1}, meeting the US Department of Energy's 2020 target for onboard hydrogen storage. Chengfeng Liao *et al.*[34] introduced an ammonia-fueled solid oxide fuel cell vehicle (NH_3-SOFCV) to address hydrogen storage challenges in new energy vehicles. A life cycle assessment (LCA) revealed that the vehicle's manufacturing phase had the highest energy consumption and CO_2 emissions, while the use phase involved lower emissions mainly from maintenance. The global warming potential (GWP) was 0.124 kg CO_2-eq per km, and ammonia utilization impacted acidification and eutrophication potentials. Extending the vehicle's life cycle and using renewable energy for ammonia production could reduce environmental impacts by up to 29%. Mohammed *et al.*[35] conducted a risk assessment on onboard hydrogen storage in hydrogen-powered vehicles exposed to fire. The study showed that increasing the fire resistance rating (FRR) of the storage tank significantly reduced risks to acceptable levels. Using UK vehicle fire data, it was found that an unprotected composite tank posed a high risk of human life loss, but this risk could be minimized with improved FRR through thermal protection. Giuseppe Pozzana *et al.*[36] explored ammonia as a fuel in a 15 kW internal combustion engine for a hybrid electric vehicle, where ammonia acts as a range extender for an onboard lithium battery pack. Hydrogen, produced by thermally decomposing ammonia at 400 °C using a specialized catalyst, is used to enhance combustion. The engine successfully managed ammonia combustion, producing water and nitrogen oxides, with a NOx emission of a maximum of 9.9 g kW^{-1} h^{-1} at 4500 rpm. However, challenges remain regarding engine performance, system reliability, and safety. Wang *et al.*[37] studied an onboard ammonia cracking system for hydrogen production in turbojet engines to mitigate hydrogen's low density issues. Their precooled engine cycle achieved a Mach number of 4.69 and significantly reduced carbon emissions by up to 94.15%. The study highlighted ammonia's superior heat sink capacity and hydrogen production rate, although system integration and managing the precooled setup remain challenging. Zhang *et al.*[38] developed advanced ruthenium-based catalysts for high-temperature ammonia decomposition. Although these catalysts enhance performance and stability at elevated temperatures, challenges such as high

operational temperatures leading to catalyst degradation and the need for durable materials persist. Wang *et al.*[39] employed nickel-based catalysts for ammonia decomposition at lower temperatures. While these catalysts are effective at lower temperatures, challenges include slower reaction rates and potential catalyst longevity issues. Guangyan Zhu *et al.*[40] evaluated ammonia-hydrogen fuel cell electric vehicles (FCEVs) as a competitive energy solution, noting their high energy density and reduced greenhouse gas emissions. However, challenges include high ammonia production costs, inefficient ammonia cracking processes, and the need for advancements in fuel cell technology. The study also highlighted issues with ammonia storage, distribution, and the environmental impact of ammonia production. Yosuke Saito *et al.*[41] developed an onboard hydrogen generation system for FCEVs using an ammonia cracker. The system, featuring a Ru/Al_2O_3 catalyst and an optimal cracking temperature of 700 °C, demonstrated higher efficiency than Ni/Al_2O_3. The compact FCEV design (3400 mm × 1480 mm × 2000 mm) achieved a 100 km range with a 10-liter ammonia cylinder and a top speed of 100 km h^{-1}. Key challenges include reducing the ammonia cracker's footprint, improving catalyst efficiency, integrating the system, and addressing the costs and environmental impacts of ammonia production.

This paper presents a comprehensive evaluation and optimization of a novel compact onboard ammonia cracker integrated with a 100-kW fuel cell for electric vehicles. It proposes a novel design featuring a hollow fibre palladium alloy membrane reactor (HFMR) module and assesses its performance in both steady-state and transient conditions for light-duty automotive fuel cell vehicles. The study focuses on designing the compact HFMR module and optimizing its arrangement to enhance the efficiency and integration of the ammonia cracker within the fuel cell system. The onboard ammonia cracker for vehicles offers several advantages over conventional FCVs carrying pressurised or liquefied hydrogen. These benefits include:

(1) It eliminates having a separate hydrogen production plant and all the CAPEX and operating cost associated with the plant

(2) Cost and safety reduction: it eliminates the need for high-pressure hydrogen storage (over 70 000 kPa), reducing costs and minimizing explosion risks and hydrogen embrittlement-related containment failures.

(3) Reduced cooling requirements: it removes the need for low-temperature refrigeration for hydrogen storage, further lowering costs.

(4) Safer refuelling stations: by dispensing only ammonia, it reduces explosion risks associated with hydrogen.

(5) Enhanced efficiency: it enables heat and energy integration between the vehicle's proton exchange membrane fuel cell (PEMFC) and the onboard ammonia cracker, improving overall thermal and process efficiency.

Despite these advantages, safety and handling challenges associated with ammonia remain a concern due to its toxic and corrosive nature. While ammonia is relatively easy to store under moderate pressure or at low temperatures, onboard systems must be designed to safely contain ammonia, protect

against leaks, and minimize exposure risks. The innovation of this process stems from the integration of a cutting-edge, compact onboard ammonia cracker module, which incorporates a hollow fibre palladium alloy membrane reactor (HFMR), alongside a 100-kW fuel cell system designed for light-duty vehicles.

2. Methodology and assumptions

2.1 Reactor and heater module arrangement

The schematic diagram and cross-sectional view for the novel onboard ammonia cracker is presented in Fig. 2(a) and (b), providing an overview of the system's operational framework. Fig. 3 and 4 showcase various cracker configurations that were rigorously evaluated during the design phase. Several arrangements were ultimately dismissed during initial screenings due to suboptimal performance or complexities in implementation. Fig. 5 illustrates the serpentine arrangement of the reactors and heaters, highlighting the strategic layout designed to enhance heat and mass transfer efficiency. This configuration is critical for optimizing the ammonia cracking process, ensuring effective thermal management and maximizing hydrogen yield.

System overview: as shown in Fig. 2a, the system operates with pure liquid ammonia at a flow rate of 115.3 liters per hour (STP). The ammonia is stored in a pressurized tank at 1000 kPa and ambient temperature. Upon entering the system, the liquid ammonia undergoes vaporization in a double pipe heat exchanger that utilizes waste heat recovered from the hydrogen product stream exiting the cracker module as part of heat integration to enhances the overall thermal efficiency of the process.

Cracker and heater module design: the cracker module is engineered using a hollow fibre palladium membrane with the details shown in Tables 1 and 2. In this configuration, ammonia gas flows through the inner fibres of the reactor, while the product stream circulates through the annular space between the outer tube and the inner fibres. This design maximizes surface area and promotes efficient heat and mass transfer.

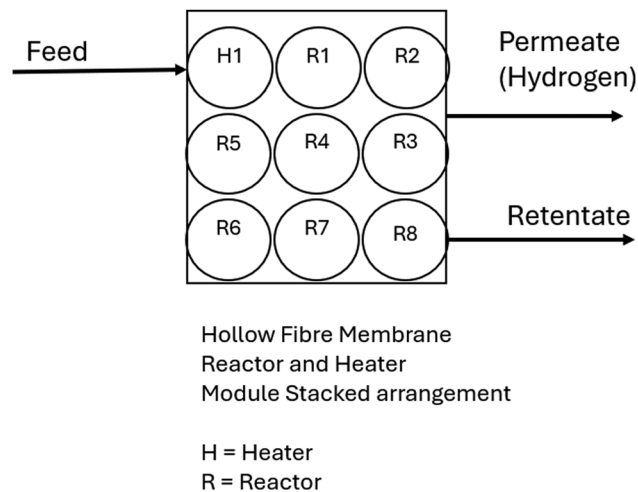Evaluated configurations: two primary reactor and heater configurations were critically assessed:

Fig. 3   3 × 3 simultaneous heating and cracking HFMR module.
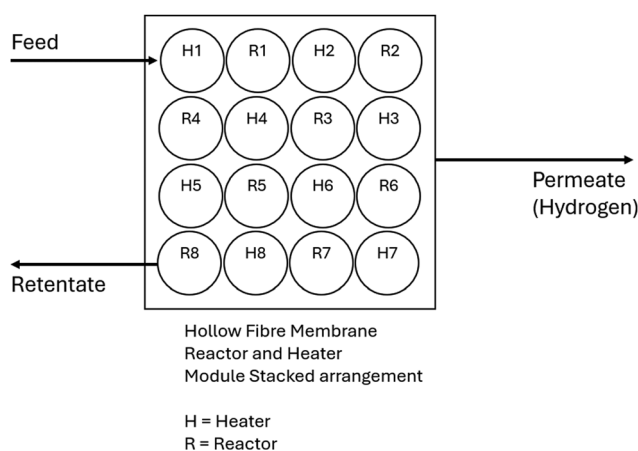

Fig. 4   4 × 4 intermediate heating and cracking HFMR module.

(1) Simultaneous cracking and heating: this configuration integrates the cracking and heating processes into a continuous operation, allowing for enhanced efficiency and reduced thermal lag (see Fig. 3). This arrangement was favoured for its
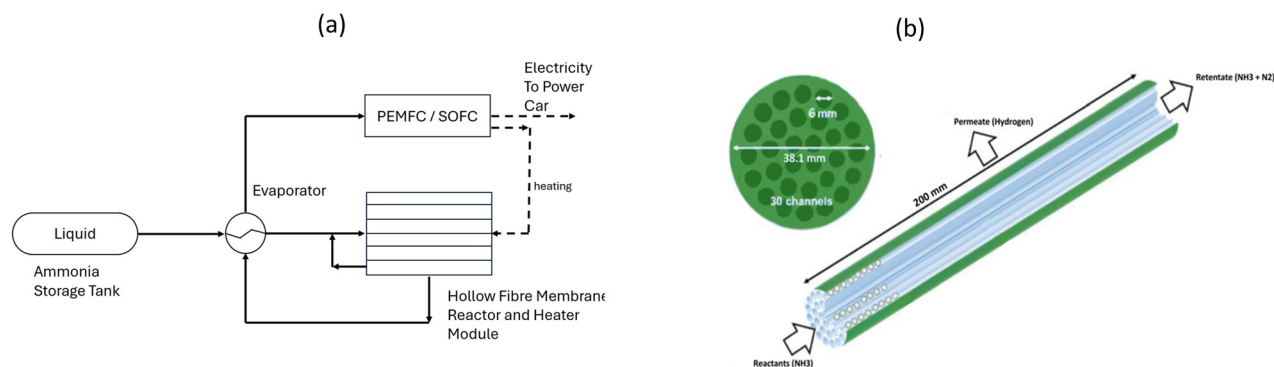

Fig. 2   (a) Schematic diagram of novel onboard ammonia cracker for light-duty automotive fuel cell vehicle, (b) cross section of one hollow fibre membrane reactor (HFMR) with 30 channels.
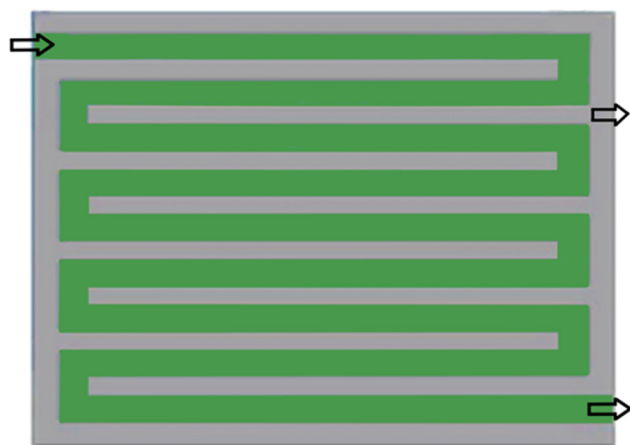
Fig. 5 Serpentine cross section arrangement of each the reactors and heaters are arranged.

potential to streamline the reaction kinetics and optimize energy use.

(2) Intermediate heating and cracking: in this method, ammonia gas is pre-heated using resistive heating before entering the cracker module for the cracking reaction (see Fig. 4). This approach facilitates improved control over the reaction temperature, potentially increasing conversion rates by ensuring that the feed gas reaches the optimal temperature prior to cracking.

Unreacted ammonia and nitrogen are channelled through additional reactors arranged in a serpentine configuration, ensuring complete reaction and maximizing hydrogen yield. The product hydrogen is then cooled in an evaporator to maintain a temperature range between 30 °C to 40 °C, making it suitable for feeding into the proton exchange membrane fuel cell (PEMFC) engine; in addition, solid oxide fuel cell (SOFC) can also be integrated with the ammonia cracker module and the heat extracted can be used for the endothermic cracking reaction. Unreacted ammonia is recycled back into the system, while nitrogen is vented, minimizing waste and enhancing process sustainability. The overall design aims to produce 72.4 cubic meters per hour (STP) of hydrogen, which is utilized to generate 100 kW of electrical power. This electrical power not only supports the operation of the PEMFC engine but also

Table 1 System and operating specifications for 3 × 3 simultaneous heating and cracking module

Parameter	Value	Units
Cracker and heater module		
Number of reactors/heaters	8	—
Reactor pressure (tube side)	800	kPa
Reactor pressure (annulus side)	300	kPa
Reactor outlet temperature	475	°C
Hollow fibre hole diameter	0.006	m
Hollow fibre length	0.2	m
Number of holes per reactor module	30	—
Hollow fibre membrane reactor diameter	0.0381	m
Membrane permeance	0.00346	mol m^{-2} s^{-1} Pa$^{-0.5}$
Membrane thickness	6	μm

Table 2 System and operating specifications for 4 × 4 intermediate heating and cracking module

Parameter	Value	Units
Cracker and heater module		
Number of reactors	8	—
Number of heaters	9	
Reactor pressure (tube side)	800	kPa
Reactor pressure (annulus side)	300	kPa
Reactor outlet temperature	600	°C
Hollow fibre diameter	0.006	m
Hollow fibre length	0.2	m
Number of holes per reactor module	30	—
Hollow fibre membrane reactor diameter	0.0381	m
Membrane permeance	0.00346	Mol m^{-2} s^{-1} Pa$^{-0.5}$
Membrane thickness	6	μm

supplies the necessary resistive heating for the cracker and heater module, creating a self-sustaining energy loop within the system.

2.2 Steady state process modelling and simulation

To evaluate the viability of various reactor and heater module configurations, a comprehensive methodology was employed using steady-state thermodynamic equilibrium and kinetic modelling with Aspen Plus software. This approach assessed key parameters such as system size, compactness, ammonia conversion efficiency, temperature requirements, and overall process performance. The model is based on a 1-D heterogeneous reactor design and utilizes the Temkin–Phyzev rate kinetics model, which has been reliably applied in previous studies to fit experimental conversion rates for ammonia decomposition reactions.[21,36,37]

Model description:

• Reactor type: the model uses a 1-D heterogeneous reactor framework, appropriate for simulating the complex interactions within the reactor system.

• Kinetics model: the rate kinetics for ammonia decomposition is represented using the Temkin–Phyzev model. This model has demonstrated accuracy in capturing the dynamics of ammonia decomposition across various studies. Table 3 shows the kinetic constants used for the hollow fibre reactor[28] modelling.

• Temperature range: for temperatures between 400 °C and 750 °C, the reaction is not constrained by equilibrium limitations.[37] In this high-temperature range, the reaction kinetics are described by a power law, which provides a suitable approximation for the rate of ammonia decomposition.

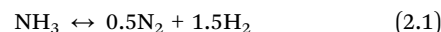## 2.3 Kinetic and key equations

(1) Reaction:

$$NH_3 \leftrightarrow 0.5N_2 + 1.5H_2 \qquad (2.1)$$

Table 3 Kinetic parameters used for hollow fibre reactor[32]

	k_0 [h^{-1}]	E_0 [kJ mol^{-1}]
S. Mazzone et al. (2021)[32]	1.2×10^8	65.2

(2) Rate expression:

The reaction rate, R is given by:[31,41]

$$R = k_{app} \left(\frac{P_{NH_3}^2}{P_{H_2}^3} \right)^{\beta} \qquad (2.2)$$

(3) Apparent rate constant:

The apparent rate constant k_{app} is defined by:[31,41]

$$k_{app} = k_{0pp} \exp\left(\frac{-E_{app}}{RT} \right) \qquad (2.3)$$

(4) Membrane flow calculation

The hydrogen flow from the retentate to the permeate side of the membrane reactor is governed by Sievert's law:[43]

$$F_{H_2.} = H_{2permeance} A_m \sqrt{P_{H2reac} - P_{H2ret}} \qquad (2.4)$$

(5) Fuel cell electric car power:

Electric power generated by a fuel cell engine is given by:[44]

$$Power = \eta_{anode} \times \eta_{FC} \times \dot{M}_{H2} \times LHV_{H2} \qquad (2.5)$$

(6) Relationship of car engine power, speed and hydrogen consumption

As per the longitudinal dynamics model,[45] power per constant speed of the car can be calculated as follows:

$$F_{stab} = a + b \cdot V + c \cdot V^2 + F_{cl} \qquad (2.6)$$

$$F_{cl} = (m + load)g \sin^{-1}\left(\tan \frac{alpha}{100} \right) \qquad (2.7)$$

$$F_{total} = ma + F_{stab} \qquad (2.8)$$

$$Power = F_{total} x V \qquad (2.9)$$

2.4 Transient modelling of the on-board ammonia cracker

Aspen Plus Dynamics software was used to carry out the transient modelling of the onboard ammonia cracker to evaluate system performance. The transient modelling evaluates the cracker performance under various operating conditions of the vehicle, including load changes, high-power scenarios, idling, acceleration, and deceleration. The analysis encompasses several critical parameters, providing a comprehensive understanding of the cracker's dynamics during simulated real-world driving conditions. To investigate the performance of the onboard ammonia cracker, a Hyundai Nexo 95-kW fuel cell vehicle had been adapted.[42] The worldwide harmonised light vehicle test procedure (WLTP) was employed to simulate realistic driving cycles, allowing for a rigorous interrogation of the transient performance of the on-board ammonia cracker.

2.4.1 Key aspects of the transient modelling. (1) Vehicle acceleration, cruising, and deceleration

The transient behaviour of the ammonia cracker is analysed in conjunction with the vehicle's acceleration, cruising, and deceleration phases. This evaluation captures how varying demand for power affects the cracking process, ensuring that hydrogen production aligns with the vehicle's performance requirements during these transitions.

(2) Transient behaviour of car power and speed *versus* time

The relationship between power demand and vehicle speed is modelled to determine how quickly the ammonia cracker can respond to changes in driving conditions. By plotting power and speed against time, insights into the responsiveness of the cracker during dynamic driving situations can be gained.

(3) Transient behaviour of car speed and ammonia consumption *versus* time

This aspect examines how the consumption of ammonia correlates with changes in vehicle speed. Understanding the consumption patterns during different driving cycles is essential for optimizing the cracker's efficiency and ensuring that sufficient hydrogen is available for fuel cell operation.

(4) Transient behaviour of car speed and hydrogen production *versus* time

Finally, the model investigates how vehicle speed influences hydrogen production rates from the ammonia cracker.

By tracking these variables over time, the performance of the hydrogen production system can be effectively evaluated against varying operational demands.

3. Results and discussions

3.1 Model validation and experimental comparisons

In our previous publication,[31] we conducted a thorough validation of the ammonia decomposition model. Further validation of the hollow fibre reactor was undertaken, building on the experimental research conducted by S. Mazzone *et al.* (2021),[32] which utilized a ruthenium-based catalyst supported on carbon xerogels (Ru-NCX). The models developed for the reactor demonstrated a strong correlation with the experimental data, as depicted in Fig. 6.

Our analysis showed that at temperatures of 400 °C and above, the accuracy of the model significantly improved, achieving discrepancies of less than 5% between model predictions and experimental outcomes. Notably, at 450 °C, we observed that ammonia conversion rates closely approached equilibrium levels, with both experimental and modelled results converging effectively.

It is essential to highlight that these validations were conducted using literature results from a small-scale laboratory setups.

Table 4 Adapted Hyundai Nexo 95-kW fuel cell car parameters[42]

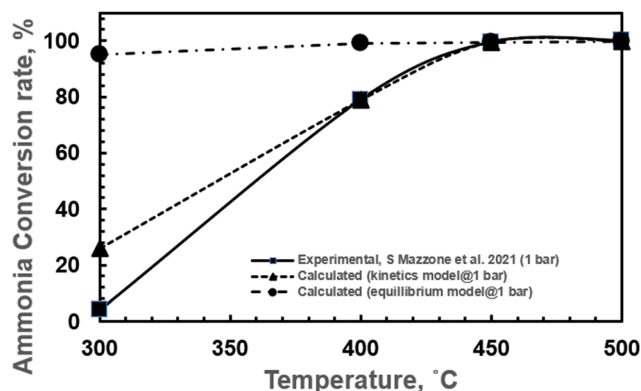| Parameter	Value	Units
Descriptions	Values	—
Max power stack	95	kW
Fuel economy	61	MPGe
Engine efficiency	65	%
Stack power density	3.1	kW L^{-1}
Fuel pressure	70	Mpa
Fuel tank capacity	6.33	kg
Car mass	2057	kg
Frontal area	2.45	m^2
Range	380	miles
Road/load constants	$a = 178.7$ N	
	$b = 0.919$ N (km h)$^{-1}$	
	$c = 0.04037$ N (km h)$^{-2}$	

Fig. 6 Conversion *vs.* temperature for experimental data (S. Mazzone *et al.* (2021)),[32] equilibrium model and kinetic model across temperatures ranging from 300 °C to 500 °C and pressures.

This methodological choice helped mitigate potential influences from various factors such as gas feed impurities, mechanical erosion, and mass transfer limitations, all of which can significantly affect catalyst activity in larger industrial reactors. However, while this controlled environment offers valuable insights, it may not fully account for the complexities and variabilities inherent in industrial-scale operations, warranting caution in extrapolating these results directly to larger systems. Future work should aim to bridge this gap by exploring how these findings can be scaled effectively within an industrial context.

3.1.1 Steady state evaluation of novel on-board ammonia cracker module (3×3 simultaneous heating and cracking module). In the 3×3 simultaneous heating and cracking process, the hollow fibre membrane reactor (HFMR) module is configured in a serpentine arrangement, effectively integrating the cracking and heating processes into a continuous operation. This innovative design enhances efficiency while minimising thermal lag. Each HFMR module operate isothermally at a temperature of 475 °C with resistive heating generated by the electricity produced by the fuel cell engine.

For a 100 kW fuel cell vehicle, as shown in Table 5, the required volume for the 3×3 simultaneous heating and cracking HFMR module is calculated to be 8.9 litres, with a total module area of 1.2 m². This compact design facilitates optimal performance in hydrogen production while ensuring effective thermal management.

Steady state analysis was carried out for the novel on-board ammonia cracker module (3×3 simultaneous heating and cracking module) shown in Fig. 2 and 3 in terms of ammonia conversion, hydrogen yield, hydrogen purity, hydrogen thermal efficiency and process thermal efficiency using eqn (3.1)–(3.3) 10;[31] where 'n' stands for relevant molar flowrates.

$$\text{Ammonia conversion} = \frac{n_{NH_{3(IN)}} - n_{NH_{3(OUT)}}}{n_{NH_{3(IN)}}} \times 100\% \quad (3.1)$$

$$\text{Hydrogen yield (\%)} = \frac{\text{Actual hydrogen produced}}{\text{Theoretical hydrogen produced}} \times 100\% \quad (3.2)$$

Table 5 Required total area, volume and process thermal efficiency for 3×3 simultaneous heating and cracking hollow fibre membrane (HFMR) module

Hollow fibre membrane reactor and exchanger module total required area, m²	Hollow fibre membrane reactor and exchanger module total required volume, litres	Process thermal efficiency, %
1.2	8.9	93.5

$$\text{Process thermal efficiency (\%)}$$
$$= \frac{\text{Molar flow of } H_{2(OUT)} \times HHV_{H_2}}{\text{Molar flow of } NH_{3(FEED)} \times HHV_{NH_3} + \text{net heating duty}} \times 100\%$$
$$(3.3)$$

As illustrated in Fig. 7, the ammonia conversion and hydrogen yield at the exit of the first reactor (R1) was calculated as 15.8%. This conversion rate increased to 99.99% by the time the reaction progressed to the final reactor (R8). The incremental increase in ammonia conversion across each reactor showcase a systematic enhancement of efficiency: R1 saw a conversion of 15.8%, which increased by 14.9% to 30.7% in R2. This trend continued with R3 achieving a conversion of 44.4% (an increase of 13.7%), followed by R4 at 57.1% (an increase of 12.7%), R5 at 68.5% (an increase of 11.4%), R6 at 78.6% (an increase of 10.4%), R7 at 88% (an increase of 10.1%), and finally R8 reaching 99.99% (an increase of 11.44%).

A crucial aspect of this system is the *in situ* removal of hydrogen generated within the reaction zones for each reactor, which is facilitated by the selective diffusion of hydrogen through a palladium membrane hollow fibre. This process enhances both hydrogen yield and ammonia conversion by shifting the reaction equilibrium forward, consistent with Le Chatelier's principle. Consequently, the reaction effectively progresses from ammonia and nitrogen towards hydrogen production, significantly boosting overall efficiency. Fig. 8(a)–(d) illustrate the performance profiles of each reactor, detailing the concentrations of ammonia, nitrogen, and hydrogen along the length of the reactors. It is evident that ammonia concentration decreases consistently across each reactor as it is converted into
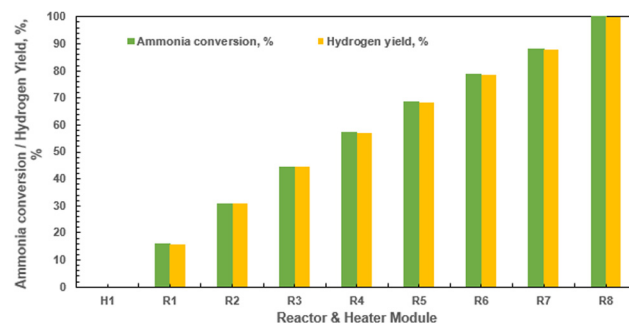

Fig. 7 Results of 3×3 simultaneous heating and cracking HFMR module showing overall ammonia conversion (%) and overall hydrogen yield at each reactor exit.

hydrogen and nitrogen, while the concentrations of both hydrogen and nitrogen increase correspondingly. The produced hydrogen is continuously removed through the hydrogen perm-selective membrane and collected in the annular space surrounding the inner fibers of the reactor.

In this system, ammonia gas flows through the inner fibres, whereas the generated hydrogen diffuses through the hydrogen perm-membrane. The unreacted ammonia and nitrogen are then channelled into additional reactors arranged in a serpentine configuration, ensuring complete reaction and optimizing hydrogen yield. At the reactor inlet, the partial pressure of hydrogen is minimal, resulting in faster reaction kinetics during the first 10% of the reactor's length. However, as hydrogen production increases, the rate of reaction slows

down, primarily due to the endothermic nature of the ammonia decomposition reaction.

Overall, the observed yields of ammonia and hydrogen at the outlets of the reactors are as follows: R1—15.8%, R2—30.7%, R3—44.4%, R4—57.1%, R5—68.5%, R6—78.6%, R7—88%, and R8—99.99%. This progressive enhancement underscores the effectiveness of the reactor design and the *in situ* hydrogen removal strategy in maximizing both ammonia conversion and hydrogen yield. Refer to ESI† for the concentration profiles across the other reactors.

3.1.2 Sensitivity analysis of 3 × 3 simultaneous heating and cracking module. The sensitivity analysis of a 3 × 3 simultaneous heating and cracking module explores the effects of reactor pressure and temperature on ammonia overall
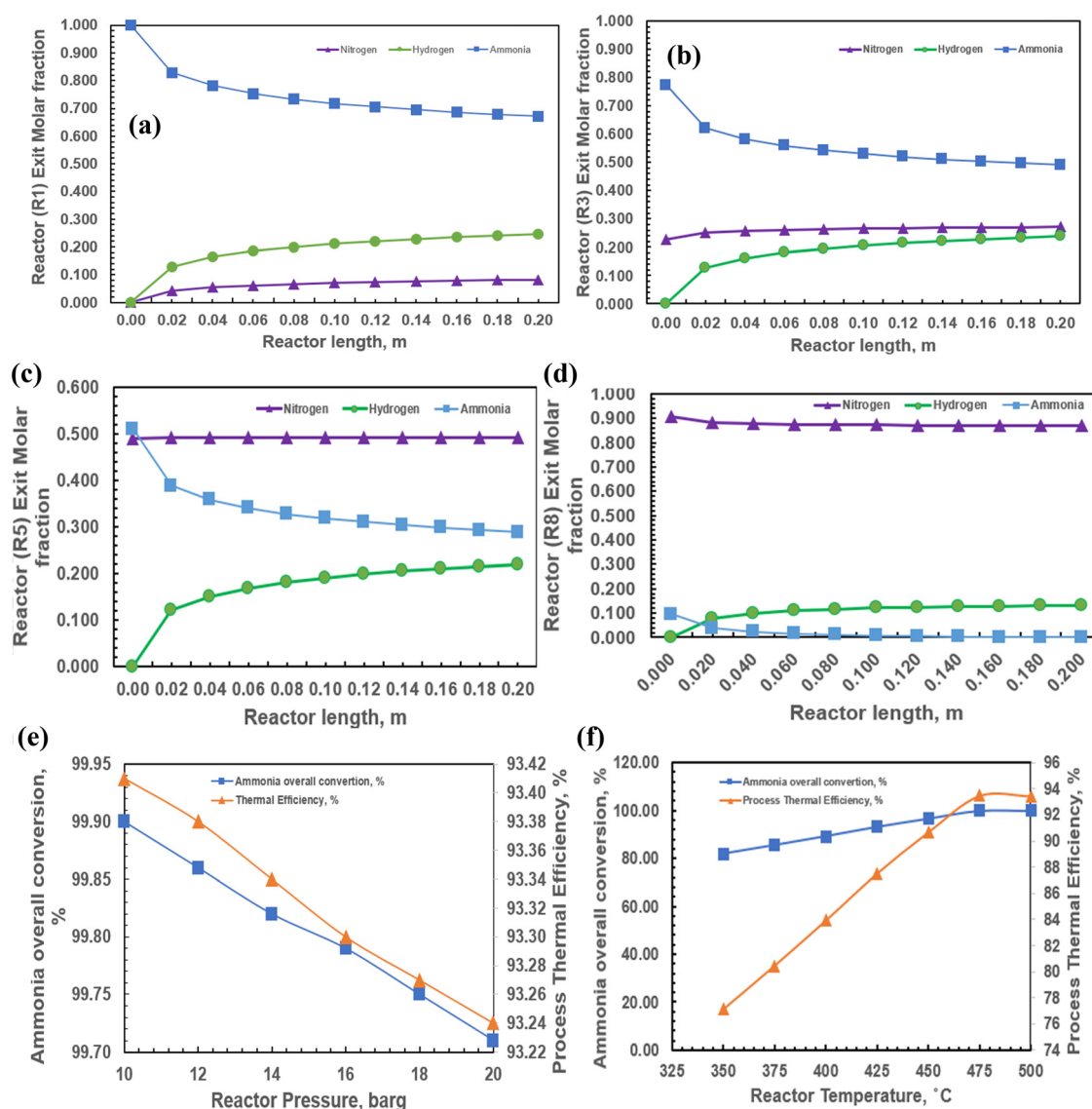
Fig. 8 (a) 3 × 3 simultaneous heating and cracking HFMR module (reactor R1 performance profile). (b) 3 × 3 simultaneous heating and cracking HFMR module (reactor R3 performance profile). (c) 3 × 3 simultaneous heating and cracking HFMR module (reactor R5 performance profile). (d) 3 × 3 simultaneous heating and cracking HFMR module (reactor R8 performance profile). (e) Sensitivity analysis of reactors pressure on 3 × 3 simultaneous heating and cracking module. (f) Sensitivity analysis of reactors temperature on 3 × 3 simultaneous heating and cracking module.

conversion and process thermal efficiency as shown in Fig. 8e and f. Understanding these dependencies is crucial for optimizing hydrogen production and ensuring the efficient operation of the onboard cracker. As shown in Fig. 8e, the impact of reactor pressure on ammonia conversion and thermal efficiency reveals a negative correlation between pressure and conversion. At 8 barg, ammonia overall conversion is approximately 99.94%, but as pressure increases to 20 barg, conversion declines to 99.71%. This trend suggests that higher pressures shift the reaction equilibrium unfavourably, reducing the extent of ammonia decomposition. The process thermal efficiency follows a similar, albeit less pronounced, downward trend, decreasing from 93.45% at 8 barg to 93.24% at 20 barg. The relatively minor drop in efficiency suggests that the system remains thermally stable at varying pressures but performs best at lower pressures where conversion is maximized. The influence of reactor temperature exhibits a significantly stronger effect on ammonia conversion as shown in Fig. 8f. At 350 °C, conversion is notably low, well below 82%, indicating insufficient thermal energy to drive the endothermic ammonia cracking reaction. As temperature increases, ammonia conversion improves steadily, reaching up to 99.94% at 475 °C. This behaviour aligns with reaction kinetics, where higher temperatures enhance reaction rates and shift equilibrium toward complete ammonia dissociation. Process thermal efficiency also improves with temperature, increasing from below 77% at 350 °C to 94% at 475 °C. This suggests that higher temperatures not only enhance hydrogen yield but also improve the overall system's thermal performance. When integrating both pressure and temperature sensitivity analyses, a clear trade-off emerges. Temperature is the dominant factor influencing ammonia conversion, with significant performance improvements seen as temperatures exceed 450 °C. However, increasing pressure negatively impacts conversion, meaning that operating at high pressures does not compensate for low temperatures. Instead, an optimal balance is required: operating the reactor at elevated temperatures of 450 °C while keeping pressure within a moderate range (8 barg) ensures near-complete ammonia decomposition with minimal thermal efficiency loss.

3.2 Steady state evaluation of novel on-board ammonia cracker module (4 × 4 intermediate heating and cracking module)

For the 4 × 4 intermediate heating and cracking process, the hollow fibre membrane reactor (HFMR) module is designed in a serpentine configuration similar to the 3 × 3 simultaneous heating and cracking module, however; intermediate electric heating is provided at the outlet of each adiabatic hollow fibre membrane reactor. Each resistive electric heater maintains an exit temperature of 600 °C, derived from the electricity generated by the fuel cell engine or heat extracted from the fuel cell engine, thereby ensuring optimal thermal conditions for the reaction.

For a 100 kW fuel cell vehicle, the volume necessary for the 4 × 4 HFMR module is calculated to be 25.6 litres, with a

Table 6 Required total area, volume and process thermal efficiency for 4 × 4 intermediate heating and cracking hollow fibre membrane (HFMR) module

Hollow fibre membrane reactor and exchanger module total required area, m^2	Hollow fibre membrane reactor and exchanger module total required volume, litres	Process thermal efficiency, %
1.5	25.6	92.8

module area of 1.5 m^2 (Table 6). As illustrated in Appendix A (ESI†), the ammonia conversion and hydrogen yield at the exit of the first reactor (R1) were initially 19.6%. This conversion rate increased dramatically, ultimately achieving 99.99% by the time the reaction reached the final reactor (R8) similar to the 3 × 3 simultaneous heating and cracking module described in Section 3.2. The incremental enhancements in ammonia conversion across each reactor highlight the efficiency of the system.

A pivotal aspect of this reactor design is the *in situ* removal of hydrogen produced within each reaction zone, facilitated by the selective diffusion through a palladium membrane hollow fibre. This mechanism enhances both hydrogen yield and ammonia conversion by shifting the equilibrium of the reaction forward in accordance with Le Chatelier's principle.

Fig. 9(a)–(d) provide comprehensive performance profiles for each reactor in the 4 × 4 intermediate heating and cracking module, showing the concentrations of ammonia, nitrogen, and hydrogen along the reactor length. It is evident that ammonia concentration consistently diminishes as it is converted into hydrogen and nitrogen, while the concentrations of both hydrogen and nitrogen increase in tandem. The results are similar to the previous 3 × 3 simultaneous heating and cracking module discussed in Section 3.2. Refer to ESI† for the concentration profiles across the other reactors (Appendix C).

3.3 Transient analysis of novel on-board ammonia cracker module

A transient analysis of the onboard ammonia cracker was conducted using Aspen Plus Dynamics software to evaluate the system's performance across a range of dynamic vehicle operating conditions. The study considered various driving phases, including deceleration, stabilization at minimum cruising speed, acceleration, full acceleration, load variations, high-power scenarios, idling, and transitions between these states. For the case study, the Hyundai Nexo, a 95-kW fuel cell vehicle, was used, and the worldwide harmonised light vehicle test procedure (WLTP) was employed to simulate realistic driving cycles.

Fig. 10(a) and (b) depict the transient behaviour of the ammonia cracker under different dynamic conditions. In particular, the analysis focuses on the system's response during deceleration, low-speed cruising, and acceleration, key phases of vehicle operation.

During the initial deceleration phase (0–4 seconds), a notable decrease in ammonia molar flowrate is observed across all reactors (Fig. 10a). This sharp decline reflects the reduced kinetics of the ammonia cracker as the system enters low-power
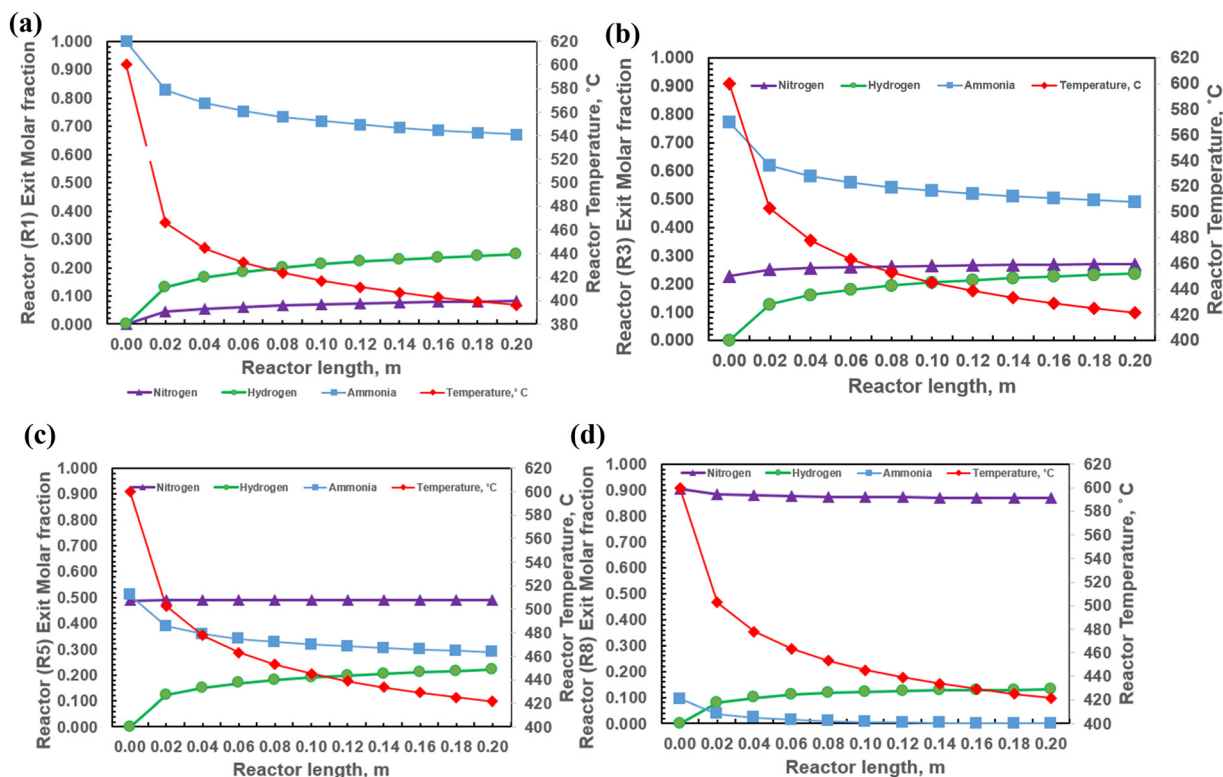
Fig. 9 (a) 4 × 4 intermediate heating and cracking HFMR module (reactor R1 performance profile). (b) 4 × 4 intermediate heating and cracking HFMR module (reactor R3 performance profile). (c) 4 × 4 intermediate heating and cracking HFMR module (reactor R5 performance profile). (d) 4 × 4 intermediate heating and cracking HFMR module (reactor R8 performance profile).

conditions. As the vehicle decelerates, the ammonia flow entering the cracker drops, resulting in decreased reactor efficiency. The hydrogen molar flowrate at the reactor outlets also decreases in tandem (Fig. 10b), indicating a corresponding drop in conversion efficiency. These reductions suggest that the cracker operates near turndown conditions, where the system struggles to maintain high efficiency under low load demands.

From 4 to 10 seconds, during the stabilization phase at minimum cruising speed, both ammonia and hydrogen flowrates stabilize. The system enters a steady-state condition, with ammonia flowrates maintaining a relatively constant level. Reactor 1 (R1) continues to exhibit the highest ammonia outlet flow, while the subsequent reactors show progressively lower flowrates. This pattern demonstrates that reactor 1 remains the

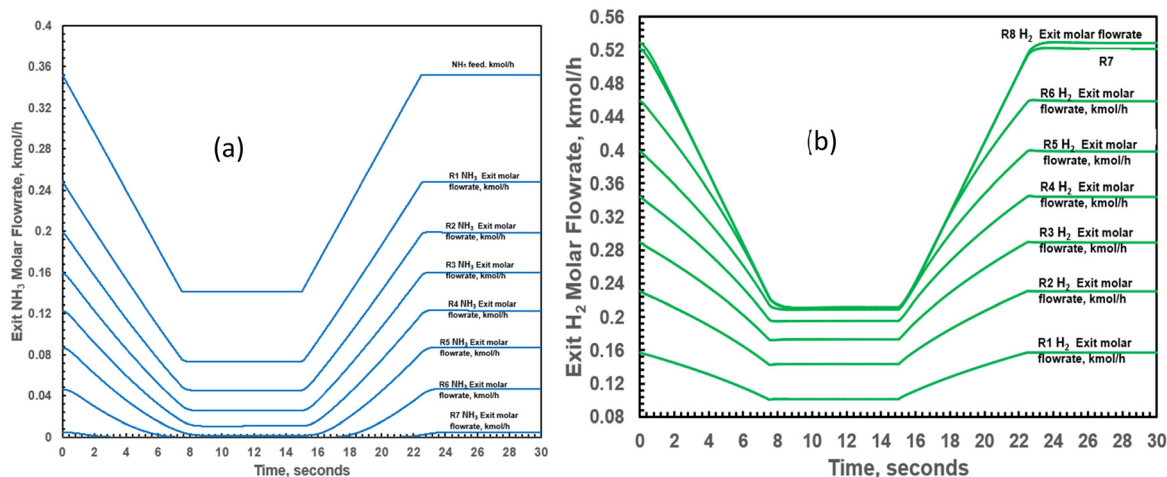Fig. 10 (a) Transient behaviour of on-board ammonia cracker during transient periods such as deceleration, cruising at minimum speed and acceleration, showing (a) reactors outlet ammonia molar flowrate. (b) Transient behaviour of on-board ammonia cracker during transient periods such as deceleration, cruising at minimum speed and acceleration, showing (b) reactors outlet hydrogen molar flowrate.

most effective in sustaining the cracking process even under reduced operational demands. Hydrogen production also stabilizes during this phase, reflecting the system's ability to maintain consistent output despite lower power requirements.

The subsequent acceleration phase (10–20 seconds) marks a dramatic shift, with both ammonia and hydrogen flowrates sharply increasing. As the vehicle accelerates, the demand for hydrogen rises, prompting the ammonia cracker to ramp up its output. The increase in ammonia flowrate drives a corresponding surge in hydrogen production, showcasing the cracker's ability to respond to higher energy demands. The system reaches its full operational capacity by 20 seconds, with both ammonia and hydrogen flowrates stabilizing at their maximum levels. This indicates that the ammonia cracker has adapted to the increased ammonia throughput, and hydrogen production now tracks the ammonia flow closely.

Overall, the transient analysis of the onboard ammonia cracker reveals its robust adaptability to varying operational conditions. The system responds efficiently to dynamic changes in demand, with ammonia and hydrogen flowrates adjusting swiftly during acceleration and deceleration phases. Notably, reactor 1 consistently outperforms the other reactors in maintaining cracking efficiency, even under lower power conditions. During the stabilization phase, the cracker maintains reliable hydrogen output at minimum cruising speeds, underscoring its ability to provide stable performance even during low-demand periods. As the system transitions to full acceleration, the rapid increase in both ammonia and hydrogen production rates highlights its capacity to meet the higher energy needs of the vehicle, ensuring a continuous and reliable hydrogen supply for fuel cell applications. The ammonia cracker's ability to transition smoothly between low and high operational states is essential for optimizing performance and maintaining fuel cell efficiency in real-world driving conditions.

3.4 Car speed and power variation, hydrogen production and ammonia consumption

The analysis of car speed variation, power requirements, hydrogen production, and ammonia consumption during the driving cycle provides critical insights into the operational behaviour of the onboard ammonia cracker system. The data, illustrated in Fig. 11 and Appendix D (ESI†), reveal distinct phases of the driving cycle: the low-speed phase (0–600 seconds), the mid-speed phase (600–1400 seconds), and the high-speed phase (1400–2000 seconds). These phases reflect the vehicle's operation under urban, suburban, and highway driving conditions, respectively, each of which significantly influences the vehicle's energy demands and the performance of the ammonia cracker system.

3.4.1 Speed phases and power requirements. The low-speed phase (0–600 seconds) as shown in Fig. 11 and Fig. S4(ESI†) is characterized by urban driving conditions, where the vehicle maintains speeds of up to 40 km h^{-1}. During this phase, power requirements are relatively modest, averaging between 5–10 kW, with occasional increases during acceleration. As the vehicle transitions to the mid-speed phase (600–1400 seconds), corresponding to suburban driving, speeds
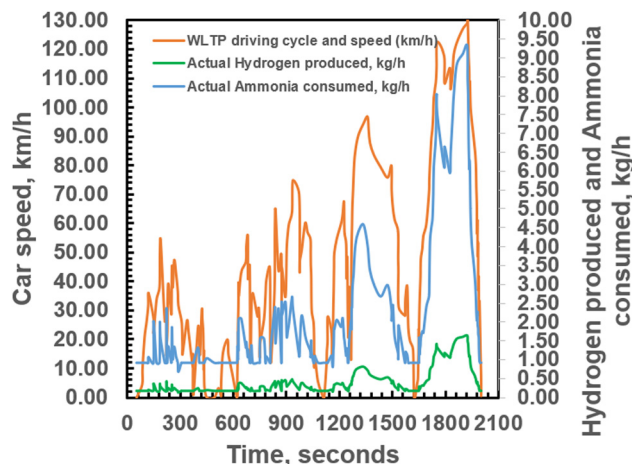

Fig. 11 Transient behaviour of on-board ammonia cracker showing the performance of the car speed; ammonia consumption and hydrogen production during different driving cycles.

fluctuate and peak at around 80 km h^{-1}. During this phase, power requirements increase to a range of 10–20 kW due to higher aerodynamic drag and the need to maintain speed. In the final high-speed phase (1400–2000 seconds), typical of highway driving, power requirements peak at approximately 36 kW, as sustained highway speeds demand significant power.

The onboard ammonia cracker system closely tracks these power demands. At low speeds, the system generates power in the range of 5–10 kW, which is adequate for urban driving. As the vehicle accelerates and enters higher-speed phases, the system increases its output, reaching a peak of approximately 36 kW during highway driving. However, a key operational feature of the system is its turndown limit, which ensures that the system maintains a minimum output of 3.5 kW, even when power demands fall below this threshold. This behaviour ensures continuous operation of the ammonia cracker, supporting system stability and efficiency at lower power demands, crucial for energy reliability.

3.4.2 Hydrogen production and ammonia consumption. Hydrogen production closely follows the variations in car speed, reflecting the changing energy demands of the vehicle. During the low-speed phase, hydrogen production is relatively low, averaging between 1.0 and 2.0 kg h^{-1}, in line with the reduced power requirements. As the vehicle accelerates into the mid-speed phase, hydrogen production increases, fluctuating between 2.0 and 5.0 kg h^{-1}, due to higher energy needs. In the high-speed phase, hydrogen production peaks at 9.0 kg h^{-1}, corresponding with the sustained high-power demands of highway driving.

In contrast, ammonia consumption remains relatively stable throughout the driving cycle, fluctuating between 0.5 and 1.5 kg h^{-1}. This stable consumption rate reflects the continuous feed of ammonia to the cracker system, ensuring a reliable hydrogen output. As the vehicle accelerates and power demands rise, ammonia consumption increases slightly, but the rate of increase is more gradual compared to the variation in hydrogen production. This steady ammonia consumption

suggests that the ammonia cracker system is designed for sustained operation, adapting to changes in hydrogen production needs without significant fluctuations in ammonia supply.

3.4.3 System behaviour and performance. The relationship between vehicle speed, hydrogen production, and ammonia consumption highlights the dynamic response of the onboard ammonia cracker system to the varying power demands of the vehicle. The system effectively adjusts to different operational states, with hydrogen production closely tracking the changes in vehicle speed and power requirements. However, a slight delay in hydrogen production during rapid acceleration phases indicates potential for optimization in the system's transient response, ensuring faster adaptation to sudden changes in power demand.

Despite this lag, the overall performance of the ammonia cracker system is robust, with the ability to consistently meet the vehicle's energy needs. The data indicate that the system can produce sufficient hydrogen under real-world driving conditions, supporting the operation of a fuel-cell vehicle. The findings confirm that ammonia is a viable hydrogen carrier, and onboard ammonia cracking technology can play a significant role in enhancing the efficiency of hydrogen-powered transportation systems. The system's ability to provide continuous, stable hydrogen output, even during transitions between driving phases, underscores its potential to contribute to the future of clean and sustainable mobility.

4. Conclusions

This work presents a comprehensive evaluation and optimization of a compact onboard ammonia cracker integrated with a 100-kW fuel cell system, specifically designed for light-duty electric vehicles. The innovative design, based around the hollow fibre palladium alloy membrane reactor (HFMR) module, demonstrates high efficiency in hydrogen production, achieving excellent ammonia conversion rates. Palladium (Pd) alloy membranes were used for hydrogen separation due to their ability to selectively permeate hydrogen at temperatures up to 987 K. Challenges such as hydrogen embrittlement, which weakens the membrane, and contaminant poisoning from impurities like water vapor, H_2S, N_2, and CO, can affect long-term stability. These issues are mitigated by alloying Pd with elements like Mo, Rh, Zr, Ru, Ag, Cu, Fe, and Ni, which enhance the membrane's mechanical strength, resistance to degradation, and protection against contaminants, making them more suitable for high-temperature applications like onboard ammonia cracking in fuel cell vehicles.

Steady-state evaluations reveal that ammonia conversion begins at 15.8% in the first reactor (R1) and increases to 99.99% by the final reactor (R8). This improvement underscores the efficacy of the *in situ* hydrogen removal mechanism facilitated by the palladium alloy membrane, which shifts the reaction equilibrium according to Le Chatelier's principle. The sequential increases in conversion rates (*e.g.*, R2 reaching 30.7%, R3 at 44.4%, and R4 at 57.1%) demonstrate systematic efficiency gains.

Two HFMR module configurations were evaluated for onboard ammonia cracking: the 3×3 simultaneous heating and cracking module and the 4×4 intermediate heating and cracking module. The 3×3 module has a compact volume of 8.9 liters and a total area of 1.2 m^2, achieving a thermal efficiency of 93.5%. Each reactor operates isothermally at a temperature of 475 °C, ensuring optimal thermal conditions while minimizing thermal lag. This compact design is highly efficient for hydrogen production in space-constrained applications. In contrast, the 4×4 module, with a larger volume of 25.6 liters and a total area of 1.5 m^2, operates adiabatically at a higher temperature of 600 °C and achieves a comparable thermal efficiency of 92.8%. While both configurations achieve 99.99% ammonia conversion, the 3×3 module is more suitable for light-duty fuel cell vehicles due to its smaller footprint and efficient integration with the vehicle's fuel cell system. The 3×3 configuration offers superior scalability advantages, ensuring high hydrogen production efficiency while minimizing thermal lag. The calculated hydrogen yield (99.9%) and process thermal efficiency (93.5%) for the onboard ammonia cracker compare favourably with our previously developed, highly efficient centralized ammonia cracking process—the novel HAVAC process.[31] The 4×4 configuration, though suitable for larger systems, is less optimal for space-limited applications.

Transient analysis further highlights the ammonia cracker's robust performance under dynamic driving conditions, using the Hyundai Nexo as a case study. Simulations under the worldwide harmonised light vehicle test procedure (WLTP) reveal trends in system performance during various driving phases. For example, during deceleration, ammonia molar flow rate and hydrogen output decrease, while a sharp increase in hydrogen production is observed during acceleration, indicating the system's adaptability to fluctuating power demands. The ammonia cracker's responsiveness ensures operational stability, meeting power needs even during high-speed driving conditions. Although hydrogen production experiences some lag during rapid acceleration, integrating a hydrogen buffer or a hybrid power source, such as a battery or capacitor, can mitigate this. This hybrid system would provide instantaneous hydrogen supply during acceleration while the ammonia cracker ramps up production, enhancing overall operational efficiency.

Safety measures are paramount when using ammonia in light-duty FCVs due to its toxic, corrosive, and flammable properties. Strict safety protocols, informed by exposure limits from organizations like the UK Health and Safety Executive (HSE) and the US Occupational Safety and Health Administration (OSHA), are essential. Continuous ammonia leak detection is critical, using sensors such as electrochemical, photoionization, and infrared technologies. These sensors, placed in strategic areas such as the passenger compartment, ammonia storage, and exhaust system, enable real-time monitoring of ammonia concentrations. Leak detection systems, corrosion-resistant materials, and automatic shutoff features reduce leak risks, and emergency protocols—such as system shutdown,

ventilation, neutralization, and egress—ensure protection in the event of a leak. Adherence to these safety measures, alongside continuous improvements in ammonia cracker design, guarantees the safe and sustainable operation of ammonia-powered FCVs.

Future research focused on heat management, temperature control within the HFMR module, optimizing transient response characteristics, and improving ammonia safety could further enhance system performance, paving the way for wider adoption of hydrogen technologies in the automotive sector.

Symbols and meaning

k_{app}	Apparent rate constant
P_{NH_3}	Partial pressure of ammonia
P_{H2}	Partial pressure of hydrogen
β	Reaction order
k_{0pp}	Pre-exponential factor
E_{app}	Activation energy
R	Universal gas constant
T	Temperature in kelvin
F_{H2}	Hydrogen molar flowrate in mol s^{-1}
$H_{2permeance}$	Pd-membrane hydrogen permeance in mol m^2 s^{-1} Pa$^{-0.5}$
$P_{H2,reac}$	Reactor pressure in pascal
$P_{H2,ret}$	Reactor annulus pressure in pascal
A_m	Area of membrane tube, in metre
η_{anode}	Percentage of feed hydrogen used at the fuel cell anode, typically a value of 0.8
η_{FC}	Efficiency of fuel cell, typically a value of 0.5
$\dot{M}_{H2}$	Mass flowrate of hydrogen in kg s^{-1}
LHV_{H2}	Lower heating value of hydrogen, typically a value of 120 MJ per kg-H$_2$
F_{stab}	Force per constant speed of the car
V	Linear speed of car
F_{cl}	Traction force
m	Mass of the car
a	Car acceleration
load	Additional load of the car in kg
g	Acceleration of gravity
alpha	Slope of the road in percentage
a, b, c	Road and load parameters constants. Refer to Table 4 for details used for the adapted Hyundai Nexo fuel cell car

Data availability

This is a statement to confirm that all data used for the "Novel Onboard Ammonia Cracker for light-duty automotive fuel cell vehicles" are accurate and can be made available upon request.

Conflicts of interest

There are no conflicts to declare.

Notes and references

1 T. Wilberforce, Z. El-Hassan, F. N. Khatib, A. Al Makky, A. Baroutaji and J. G. Carton, et al., Developments of electric cars and fuel cell hydrogen electric cars, Int. J. Hydrogen Energy, 2017, **42**(40), 25695–25734.

2 T. R. Hawkins, B. Singh, G. Majeau-Bettez and A. H. Strømman, Comparative environmental life cycle assessment of conventional and electric vehicles, J. Ind. Ecol., 2013, **17**(1), 158–160.

3 S. A. Hernandez and N. J. Clark, Sustainability and electric vehicles: A review of the environmental and economic benefits, Energy Rep., 2022, **8**, 2806.

4 B. K. Sovacool and J. Hafner, The challenges of EV adoption: A review of the literature, Renewable Sustainable Energy Rev., 2019, **105**, 217–226.

5 H. L. Breetz, K. McCormick and S. Nair, Barriers to the widespread adoption of electric vehicles: Insights from a review of recent literature, Transp. Res. A: Policy Pract., 2018, **114**, 32–44.

6 X. Zhang, Y. Wang and X. Li, Impact of charging infrastructure on the adoption of electric vehicles: A comprehensive review, Renewable Sustainable Energy Rev., 2021, **135**, 110389.

7 R. Klaeboe and A. Hauge, Investigating the impact of fast charging on EVs: A case study of Norway, Transp. Policy, 2019, **78**, 1–10.

8 R. Faria, P. Marques and P. Moura, Assessing the distribution and accessibility of electric vehicle charging infrastructure, J. Cleaner Prod., 2020, **273**, 123161.

9 U.S. Department of Energy. Electric Vehicle Charging Infrastructure. Available from: **https://www.energy.gov/eere/electricvehicles/electric-vehicle-charging-infrastructure**.

10 N. S. Rajan and V. Sundararajan, Geospatial analysis of electric vehicle charging infrastructure and its impact on adoption, Transp. Res. D: Transp. Environ., 2021, **97**, 102936.

11 International Energy Agency. The Future of Hydrogen: Seizing Today's Opportunities. 2020.

12 P. Mock and Z. Yang, The Impact of Battery Electric Vehicles and Hydrogen Fuel Cell Vehicles on the Transport Sector, Energy Policy, 2022, **168**, 113128.

13 Toyota Motor Corporation. The Hydrogen Fuel Cell Vehicle. Available from: **https://www.toyota-global.com/innovation/environmental_technology/fuel_cell/**.

14 J. M. Ogden and C. Yang, A Hydrogen-Fueled Vehicle with Fast Refueling and a Long Range: A Review, J. Power Sources, 2009, **187**(1), 191–198.

15 J. C. Jansen and T. Sanders, Hydrogen Storage Technologies: A Review, Energy Rep., 2021, 7, 114–127.

16 Hyundai Motor Company. Hydrogen Fuel Cell SUV. Available from: **https://www.hyundai.com/worldwide/en/eco/nexo**.

17 L. Schlapbach and A. Züttel, Hydrogen-storage materials for mobile applications, Nature, 2001, **414**(6861), 353–358.

18 A. Züttel, Hydrogen storage methods, Naturwissenschaften, 2004, **91**(4), 157–172.

19 International Energy Agency. Global Hydrogen Review 2024. 2024.

20 M. Mullan, D. Harries and K. Brunner, Electric Vehicle Charging Infrastructure: A Comparison with Hydrogen Refuelling Stations, *Transp. Policy*, 2019, **74**, 232–241.

21 Y. Wang and J. Zhang, High-Pressure and Cryogenic Hydrogen Storage: Technologies and Challenges, *Int. J. Hydrogen Energy*, 2024, **49**(12), 6721–6736.

22 K. Yoshida, S. Matsumoto and T. Saito, Ammonia as a Hydrogen Carrier: Current Status and Future Prospects, *Energy Rep.*, 2022, **8**, 368–382.

23 International Renewable Energy Agency, *Global hydrogen trade to meet the 1.5 °C climate goal: Part II – Technology review of hydrogen carriers*, International Renewable Energy Agency, Abu Dhabi, 2022.

24 F. Jiao and B. Xu, Electrochemical Ammonia Synthesis and Ammonia Fuel Cells, *Adv. Mater.*, 2019, **31**(31), e1805173.

25 C. Makhloufi and H. N. Khatib, Large-scale decomposition of green ammonia for pure hydrogen production, *Int. J. Hydrogen Energy*, 2021, **46**(70), 34777–34787.

26 J. Andersson and S. Godefroy, Large-scale storage of hydrogen, *Int. J. Hydrogen Energy*, 2019, **44**(23), 11901–11919.

27 T. Saito and T. Nakajima, Ammonia as a Hydrogen Carrier: Opportunities and Challenges, *Renewable Sustainable Energy Rev.*, 2023, **169**, 112488.

28 D. Gordon, Q. Zhao and M. McMahon, Green Ammonia Production: Advances and Challenges, *Renewable Sustainable Energy Rev.*, 2023, **77**, 123–139.

29 R. Kumar, S. Ali and A. Singh, Innovations in Ammonia Storage Technologies for Automotive Applications, *J. Storage Mater.*, 2024, **39**, 100456.

30 X. Li, Y. Zhang and J. Lin, A Comprehensive Review of Ammonia Cracking Technologies for Hydrogen Production, *Renewable Sustainable Energy Rev.*, 2023, **171**, 112752.

31 C. Eluwah, P. S. Fennell, C. J. Tighe and A. A. Dawood *A novel technological blue hydrogen production process: industrial sorption enhanced autothermal membrane (ISEAM)*. 2023.

32 S. Mazzone, A. Campbel, G. Zhang and F. R. García-García, Ammonia cracking hollow fibre converter for on-board hydrogen production, *Int. J. Hydrogen Energy*, 2021, **46**(70), 37697–37704.

33 L. Zhai, C. Shek Wong, H. Zhang, P. Xiong, X. Xue and Y. Lun Ho, *et al.*, From lab to practical: An ammonia-powered fuel cell electric golf cart system, *Chem. Eng. J.*, 2023, **452**, 139390.

34 C. Liao, Y. Tang, Y. Liu, Z. Sun, W. Li and X. Ma, Life cycle assessment of the solid oxide fuel cell vehicles using ammonia fuel, *J. Environ. Chem. Eng.*, 2023, **11**(5), 110872.

35 M. Dadashzadeh, S. Kashkarov, D. Makarov and V. Molkov, Risk assessment methodology for onboard hydrogen storage, *Int. J. Hydrogen Energy*, 2018, **43**(12), 6462–6475.

36 G. Pozzana, N. Bonfanti, S. Frigo, P. Dario, V. Mattoli and M. Ragnoli *A Hybrid Vehicle Powered by Hydrogen and Ammonia*. SAE Technical Paper 2012-32-0085. 2012.

37 C. Wang, J. Fang, J. Xu, C. Ha, J. Xu, C. Dang, H. Liu, C. Li, C. Li, X. Xiu, Z. Liu, Y. Shen, J. Qin and J. Shao, Performance evaluation and optimization for a novel supersonic precooled engine based on hydrogen production technology from ammonia cracking, *Int. J. Hydrogen Energy*, 2024, **52**, 857–871.

38 Y. Zhang, J. Li and X. Wang, High-temperature catalysts for ammonia cracking: Performance and stability, *J. Catal.*, 2024, **416**, 23–36.

39 X. Wang, Q. Zhao and Y. Liu, Low-temperature nickel-based catalysts for ammonia decomposition, *Appl. Catal., A*, 2023, **654**, 118579.

40 G. Y. Zhu, L. Min, Y. Zhao, W. Wang, M. Wang and Q. Li, *et al.*, Comprehensive competitiveness assessment of ammonia-hydrogen fuel cell electric vehicles and their competitive routes, *Energy*, 2023, **285**, 1294711.

41 Y. Saito, T. Nohara, Y. Aoki and T. Saika, Hydrogen generation system with ammonia cracking for a fuel-cell electric vehicle, *SAE Int.*, 2009, 2009-01-1901.

42 J. Sery and P. Leduc, Fuel cell behavior and energy balance on board a Hyundai Nexo, *Int. J. Engine Res.*, 2022, **23**(5), 709–720.

43 R. Ao, R. Lu, G. Leng, Y. Zhu, F. Yan and Q. Yu, A review on numerical simulation of hydrogen production from ammonia decomposition, *Energies*, 2023, **16**(2), 921.

44 C. Eluwah, P. S. Fennell, C. J. Tighe and A. A. Dawood, A novel technological blue hydrogen production process: industrial sorption enhanced autothermal membrane (ISEAM), *Energy Adv.*, 2023, **2**(9), 1476–1494.

45 A. Cutillo, S. Specchia, M. Antonini, G. Saracco and V. Specchia, Diesel fuel processor for PEM fuel cells: Two possible alternatives (ATR versus SR), *J. Power Sources*, 2006, **154**(2), 379–385.